Received: 14 September 2024 | Revised: 12 December 2024 | Accepted: 13 February 2025 | Published online: 6 March 2025

Journal of Optics and Photonics Research
2025, Vol. 00(00) 1–8
DOI: 10.47852/bonviewJOPR52024337

RESEARCH ARTICLE

# Photonics-Driven Characterization of Highly Energetic Heavy Ion-Induced Modifications in GaAs Single Crystals Using Au and I Ions

**Habib Abdurahman Arebu[1],* and Omar Abdulsahib Saleh[1]**

[1]*Department of Physics, King Fahd University of Petroleum and Minerals, KSA*

**Abstract:** Gallium arsenide (GaAs) (100) samples were irradiated with 1.16 GeV Au ions and 30 MeV I ions at room temperature. The impact of ion fluences, ranging from $5 \times 10^{10}$ to $2.5 \times 10^{12}$ Au ions cm$^{-2}$ and $7 \times 10^{11}$ to $1 \times 10^{14}$ I ions cm$^{-2}$ at a 75° incident angle, on the surface morphology and structural properties of the irradiated GaAs samples was investigated. Advanced characterization techniques, such as Atomic Force Microscopy and micro-Raman spectroscopy, were employed for an in-depth analysis. The results indicated no formation of nanostructures on the irradiated surfaces. Raman analysis at room temperature showed softening of optical phonons due to phonon confinement at the surface, along with a downward shift in the LO and TO phonon modes for both I and Au-irradiated GaAs samples. These results are essential for understanding the photonic and optical characteristics of GaAs when subjected to heavy ion irradiation. They are analyzed in the context of ion-matter interactions in the MeV range, providing valuable insights into the optical responses and phonon behavior in altered semiconductor materials.

**Keywords:** hillocks, nanostructure, ion irradiations, swift heavy ion, ion beam

## 1. Introduction

Ion beam technology constitutes a significant research domain with broad implications in science and engineering, particularly in the characterization and modification of materials properties. Its application spans various areas, and its utilization for altering material properties was initially introduced by the discovery of semiconducting materials like silicon [1]. Subsequently, the microelectronics industry adopted ion beam approach as part of technological methods and hence evolving it into as a crucial component across industries requiring precise manufacturing [2].

Over the years, as the demand for new materials for diverse applications has grown, researchers and scientists have increasingly explored the use of this technology for material modifications. Ion beam experiment utilizing SHI represents an advanced technique in materials science and engineering, involving the controlled exposure of materials to high-energy ions, specifically those with high mass and velocity. Swift heavy ions (SHIs) typically refer to ions with energies in the MeV (mega-electron Volt) range. This process significantly modifies the physical properties of materials at the atomic and microscopic levels. Similarly, a highly charged ion beam can bring about similar changes without damaging the bulk of the material.

SHIs can induce significant damage in III–V binary and ternary semiconductors, impacting their structural and electronic properties. III–V semiconductors are compounds composed of elements from Group III (e.g., Ga, In) and Group V (e.g., As, P) of the periodic table. These materials are crucial in the field of electronics and optoelectronics due to their unique properties. The explanation of damage in semiconductors caused by SHIs differs from that in metals or insulators [3]. In semiconductors, impurities play a crucial role, with defects and dislocations being key driving factors. Unlike semiconductors, insulators are more susceptible to damage induced by SHIs [4, 5]. To generate an ion track in a semiconductor, a specific minimum electronic energy loss is necessary.

In materials such as InP, InAs, InSb, and GaSb, subjected to SHIs like Xe, Au, and Pb, approximately 19 keV/nm of electronic energy deposition is needed to make an ion track. However, in the case of Si, Ge, and gallium arsenide (GaAs) irradiated with carbon clusters in the MeV range, a significantly higher electronic energy deposition, typically at least 50 keV/nm, is needed to produce an amorphous track [6–8]. It is effectively explained the creation of ion track and damage III–V binary semiconductor. Compared with InP, InSb is vulnerable to SHI-induced damage. Under SHI irradiation, GaP and GaAs are undamaged but InAs and GaInAs show little damage. The first description of Ion-induced damage and amorphization for InP is described by [9]. Since then, a lot of characterization techniques are employed, mainly Rutherford back-scattering spectroscopy.

The creation of hillocks in ceramics involves the transformation of the material's surface and its structure due to the energy transferred from the ions to the material. This process can lead to the creation of amorphous or crystalline hillocks, depending on whether the ceramics are amorphizable or non-amorphizable. In amorphizable ceramics, both ion tracks and hillocks tend to be amorphous, indicating a homogeneity along the ion paths and local melting due to the high-energy transfer. In contrast, non-amorphizable ceramics exhibit crystalline hillocks, suggesting a recrystallization process following the initial melting [10–12].

*Corresponding author: Habib Abdurahman Arebu, Department of Physics, King Fahd University of Petroleum and Minerals, KSA. Email: g202113610@kfupm.edu

© The Author(s) 2025. Published by BON VIEW PUBLISHING PTE. LTD. This is an open access article under the CC BY License (https://creativecommons.org/licenses/by/4.0/).

While ion-induced modifications have been extensively studied and are well understood in insulating materials, intermetallic compounds, and certain metals, the exploration of ion-induced damage in semiconductors remains relatively limited. This gap underscores the importance of further research in the field of semiconductor photonics. A detailed and comprehensive understanding of the mechanisms governing defect creation in semiconductors following ion irradiation is essential for driving advancements in semiconductor technology. Such knowledge is crucial for enhancing the reliability, efficiency, and overall photonic performance of electronic and optoelectronic devices. It also paves the way for innovative applications in fields such as microelectronics, photonics, and optoelectronics. In this study, we focus on the ion-induced modifications in a single-crystal GaAs semiconductor, employing various advanced photonic characterization techniques to unravel the complexities of ion-induced damage in semiconductor materials.

The number of ion tracks per square centimeter, synonymous with fluence (ions/cm$^2$) [13], is a key parameter in photonic studies of ion-matter interactions. In certain semiconductor materials such as InP, InAs, GaSb, and InSb, the creation of amorphous ion tracks has been observed, which directly influences their optical properties. This threshold, critical for inducing significant photonic changes, may not be achieved with a single ion in specific semiconductors like Si and GaAs. However, in materials such as Si, Ge, and GaAs, amorphous tracks can be readily created by employing SHIs with sufficiently high electronic energy deposition. These modifications are of particular interest in photonics, as they can lead to significant alterations in the material's optical absorption, scattering, and luminescence properties, which are essential for the development of advanced photonic and optoelectronic devices [14, 15].

By implanting ions into GaAs, the refractive index of the material can be locally modified, enabling the creation of optical waveguides. Additionally, defects introduced by ion irradiation can be used for quantum applications, such as creating single-photon emitters for quantum cryptography. For photonic applications, precise control over Se is necessary to create the desired modifications without compromising the material's overall performance [16–19].

In addition to defect formation, ion implantation can also introduce new elements into the material that alter its optical properties. For example, by implanting dopants such as phosphorus, nitrogen, or oxygen into a semiconductor or dielectric, the chemical composition can be modified, resulting in a shift in the refractive index. This approach is widely used in the fabrication of optical fibers and integrated photonic circuits, where a controlled gradient in refractive index is necessary to confine and guide light through the desired paths [20, 21].

One of the key advantages of ion implantation for refractive index modification is its ability to create highly localized and precise changes. Ion implantation allows for sub-micron scale modifications, which is critical for modern photonic devices that require miniaturization and integration. This level of control makes it possible to fabricate complex optical circuits and photonic crystals with intricate patterns of refractive index variation, enabling advanced light manipulation and signal processing capabilities. When high-energy ions penetrate the surface of a material, they displace atoms and create vacancies, interstitials, or other defect structures. These structural changes can lead to variations in the material's density or electronic band structure, both of which affect the refractive index. By carefully controlling the ion species, energy, and dose, engineers can design regions with precise refractive index changes, forming the core and cladding of waveguides or other photonic elements [22, 23].

Ion implantation is a pivotal technique in photonics, enabling precise control over material properties at the nanoscale for applications like waveguide creation, quantum emitter development, and refractive index manipulation. During this process, ions lose energy through two primary pathways: electronic energy loss (Se) and nuclear energy loss (Sn). Se occurs due to interactions with the material's electrons, such as ionization, excitation, or electron-hole pair formation, and it becomes dominant at higher ion velocities or energies.

This mechanism is particularly important for applications such as generating color centers in materials like diamond or silicon carbide and modifying the electronic structure for waveguide fabrication. On the other hand, Sn results from collisions between ions and the target nuclei, causing atomic displacements and damage cascades. It is more prominent at lower ion velocities and is essential for inducing structural changes, such as refractive index modifications or defect engineering. Achieving the right balance between Se and Sn is crucial, as it determines the depth and type of material alterations. A higher Se-to-Sn ratio is ideal for electronic excitation with minimal lattice disruption, which is beneficial for semiconductor doping, while a higher Sn-to-Se ratio is suited for creating structural changes like damage-induced waveguides.

GaAs with ion-implanted modifications are crucial in the development of integrated photonic circuits, where light generation, manipulation, and detection occur on a single chip. The ability to tailor the optical and electronic properties of GaAs through ion implantation allows for the integration of lasers, modulators, detectors, and waveguides into a compact and efficient photonic platform. Additionally, GaAs's high electron mobility and direct bandgap make it ideal for high-speed and high-frequency applications, such as in optical communication systems and optoelectronic devices. The precision and flexibility offered by ion implantation enable the development of photonic circuits with high performance, scalability, and functionality [24, 25].

## 2. Experimental Method

In our study, we employed a 10 mm × 10 mm, 0.5 mm thick GaAs single crystal from MTI Corporation. The irradiations were conducted at room temperature with the ion beam directed normally. The SHI bombardment involved 197 Au and 126.90 I ions with a specific kinetic energy of 5.9 MeV/nucleon and 30 MeV/nucleon, respectively, and was performed at the Universal Linear Accelerator at GSI Darmstadt, Germany. The ion fluence ranged from $5 \times 10^{10}$ ions/cm$^2$ to $2.5 \times 10^{12}$ ions/cm$^2$, with precise monitoring through the measurement of the electronic signal from an Al-foil detector placed in front of the crystals was meticulously calibrated using a Faraday cup, a critical step to ensure accurate fluence determination for photonic applications. Additionally, the ion fluence was cross-verified offline through ion track etching in polycarbonate films irradiated under identical beam parameters, providing a reliable benchmark for photonic material studies.

The ion beam maintained a homogeneity of 10% to 20% across the sample holder region (40 × 40 mm$^2$), ensuring uniform ion distribution critical for consistent photonic property measurements. Post-irradiation, the samples were meticulously analyzed using atomic force microscopy to map nanoscale surface modifications, which directly influence the material's photonic characteristics. Furthermore, Raman spectroscopy, a pivotal photonic tool, was employed to investigate the optical phonon modes, providing insights into the ion-induced modifications at

**Table 1**
**Ion beam parameter calculated using SRIM 2013 code**

| Ion species | Kinetic energy E(MeV) | Electronic energy loss dE/dx (keV/nm) | Nuclear energy loss dE/dx (keV/nm) | Ion range (µm) | Mean energy loss E/R (MeV/µm) |
|---|---|---|---|---|---|
| $Au^{197}$ | 1162.3 | 34.1 | 4.94 | 45.8 | 25.4 |
| $I^{126}$ | 30 | 7.095 | 0.37 | 6.56 | 4.57 |

the phonon level. These techniques together offer a comprehensive photonic characterization of the irradiated GaAs, essential for understanding the interplay between ion irradiation and photonic material properties. Table 1 shows the ion beam parameters calculated using the SRIM 2013 code for a kinetic energy of 1162.3 MeV revealing significant details about the ion's interactions with the material. The electronic energy loss (dE/dx) is 34.1 keV/nm, reflecting the amount of energy the ion loses due to electron interactions within the material. The nuclear energy loss is 4.94 keV/nm, representing energy transfer to the atomic nuclei. The ion's range, or the distance it travels before coming to rest, is 45.8 µm. The mean energy loss (E/R) is calculated to be 25.4 MeV/µm, which provides an average measure of energy loss per unit distance traveled. For an ion with a kinetic energy of 30 MeV, the electronic energy loss decreases to 7.095 keV/nm, while the nuclear energy loss is significantly lower at 0.37 keV/nm. The ion range in this case is reduced to 6.56 µm, and the mean energy loss is 4.57 MeV/µm. These parameters collectively illustrate how the ion's energy deposition varies with its kinetic energy and provide insight into its penetration depth and interaction mechanisms within the material.

## 3. Results and Discussions

According to SRIM simulations, as presented in Figure 1, the electronic energy loss (Se) in GaAs irradiated with 1162.3 MeV Au ions is estimated at 34.1 keV/nm. Over 90% of the ion track is dominated by electronic energy loss, whereas nuclear energy loss (Sn) becomes important only close to the end of the ion penetration depth. Figure 2 depicts the relationship between ion kinetic energy and energy losses, clearly demonstrating that nuclear energy losses dominate at the beginning of the ion track, reaching a maximum known as the Bragg peak, before electronic energy losses take over. Similarly, Figure 3 shows the electronic and nuclear energy losses for GaAs irradiated with I ions, with Se recorded at 7.09 keV/nm and Sn at 0.37 keV/nm. Finally, Figure 4 illustrates the variation of ion kinetic energy with energy losses for I ions, again highlighting that nuclear energy losses dominate near the beginning of the ion track at the Bragg peak, after which electronic energy losses gradually become predominant.

The reason behind nuclear energy losses is dominant for Figures 1 and 4 because the velocity of the ion is relatively slow as it initially interacts with the target material. In this phase, the ion has a higher probability of colliding with atomic nuclei in the target, leading to significant energy transfer through elastic collisions. As the ion continues to penetrate deeper, its velocity increases due to acceleration, and electronic energy losses begin to dominate. In this later phase, the ion interacts primarily with the target's electrons, leading to processes like excitation and

**Figure 1**
**Energy loss as a function of penetration depth for GaAs irradiated with swift Au ion**

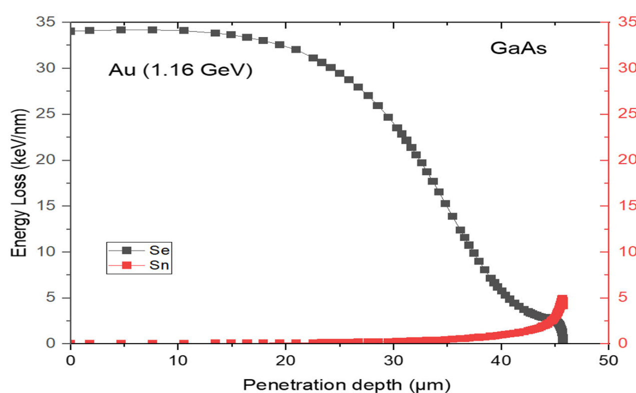


**Figure 2**
**Energy loss as a function of Ion kinetic energy for GaAs irradiated with swift Au ion**

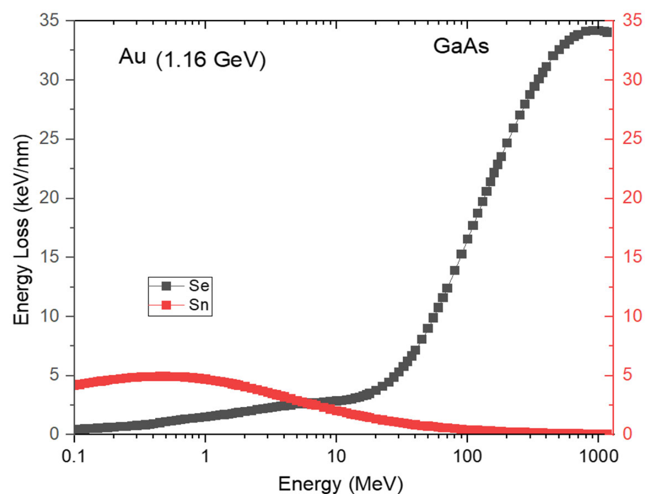


**Figure 3**
**Energy loss as a function of penetration depth for GaAs irradiated with swift I ion**

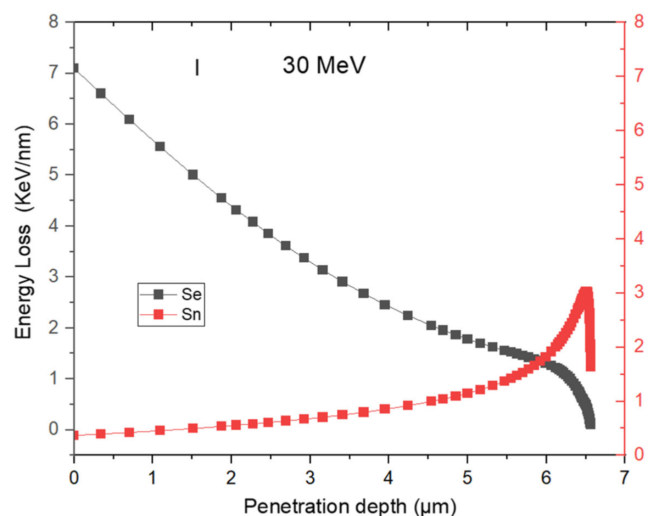

**Figure 4**
**Energy loss as a function of Ion kinetic energy for GaAs irradiated with swift I ion**

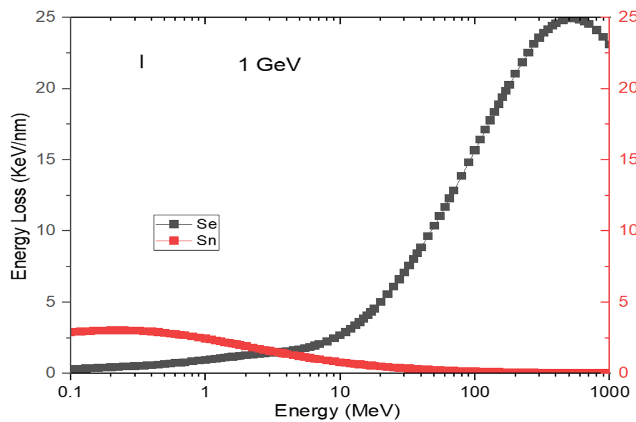


ionization. Therefore, the dominance of nuclear energy losses at the start of the track is attributed to the low initial ion velocity and the resulting higher efficiency of energy transfer to nuclei. Moreover, the electronic and nuclear energy losses intersection point signifies the transition between these two dominant energy loss mechanisms.

When the electronic energy loss is around 20 keV/nm, the development of tracks based on the ion fluence, meaning that not every incident ion creates a visible track, and some pre-damage may be required for track formation [16]. Unlike other semiconductors, GaAs did not exhibit amorphous tracks under irradiation with monoatomic ion beams. However, such tracks were readily created when MeV cluster ions with higher electronic energy loss were used [17–19]. To create the visible track the value of electronic energy losses should be high about (50 keV/nm). In our study, the value of electronic energy losses Se of 1.16 GeV Au ion in GaAs is 34.1 keV/nm, while the nuclear energy losses Sn is 4.94 keV/nm.

Thus, the Se value is 6.9 times higher than Sn. High electronic energy often results in the energy being quickly dissipated through electron-electron interactions and electron-phonon interactions, which do not significantly contribute to the localized modification of the GaAs surface [20] which is shown in Figure 5. Moreover, the roughness value for the fluence $2.5 \times 10^{12}$, $1 \times 10^{11}$, and $5 \times 10^{10}$ is found to be 6.712 nm, 5.016 nm, and 3.166 nm respectively. And the roughness value is increased with the ion fluence. Similarly in Figure 6, I-irradiated GaAs sample has a roughness value of 5.42 nm, 5.98 nm, and 7.82 nm for the fluency $1 \times 10^{12}$, $7 \times 10^{11}$, $1 \times 10^{14}$ respectively.

Utilizing the TRIM-2013 software, the path of I ions within the GaAs material is depicted in Figure 7 and its pentation depth is 6.56 µm. Similarly, the Au ion path within the GaAs material is presented in Figure 8. The penetration depth for the AU ion is 45.8 µm.

Figures 9 and 10 show vacancy distributions and energy loss for GaAs irradiated with 1162.3 MeV AU and 30 MeV I ions.

Raman spectroscopy, known for its sensitivity to atomic-scale disorder, can offer valuable insights into the structural changes occurring on ion-irradiated surfaces. In III–V semiconductors like GaAs, the first-order Raman spectrum usually features two distinct Raman modes, associated with the longitudinal optical (LO) and transverse optical (TO) phonons, which correspond to the center of the Brillouin zone. Figure 8 presents the Raman spectra for both unirradiated and AU-irradiated GaAs samples. In pristine GaAs spectrum, the LO mode appears at 292.401 $cm^{-1}$, while the TO mode is observed at 268.479 $cm^{-1}$.

The Raman spectra of AU-irradiated GaAs samples exhibit a downward shift in both the LO and TO phonon peaks. For example, as illustrated in Figure 11, at ion fluences of $5 \times 10^{12}$ ions $cm^{-2}$ and $1 \times 10^{12}$ ions $cm^{-2}$, the LO and TO peaks shifted to 281.45 $cm^{-1}$ and 258.60 $cm^{-1}$, respectively, representing a

**Figure 5**
**Atomic force microscopy images of GaAs surface irradiated by 1.16 GeV Au ions at various Ion fluences: (a) $2.5*10^{12}$, (b) $1*10^{11}$, (c) $5*10^{10}$**

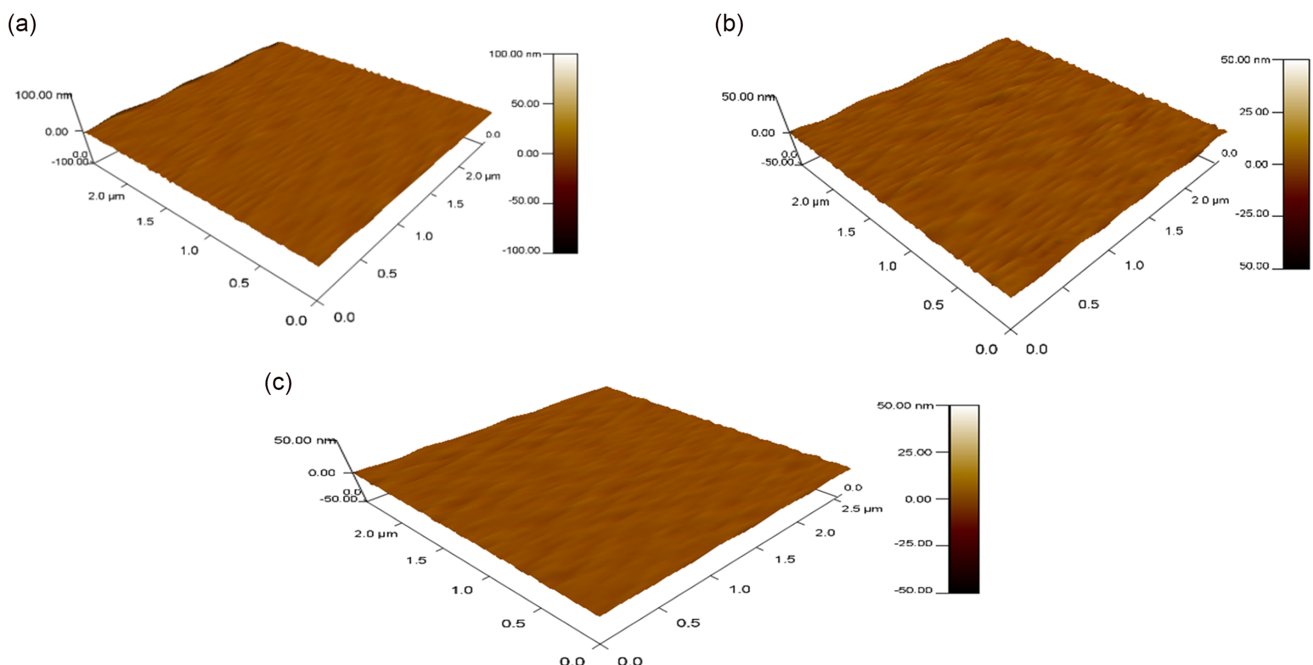

**Figure 6**
**Atomic force microscopy images of GaAs surface irradiated by 30 MeV I ions at various Ion fluences: (a) 1*10$^{12}$, (b) 7*10$^{11}$, (c) 1*10$^{14}$**

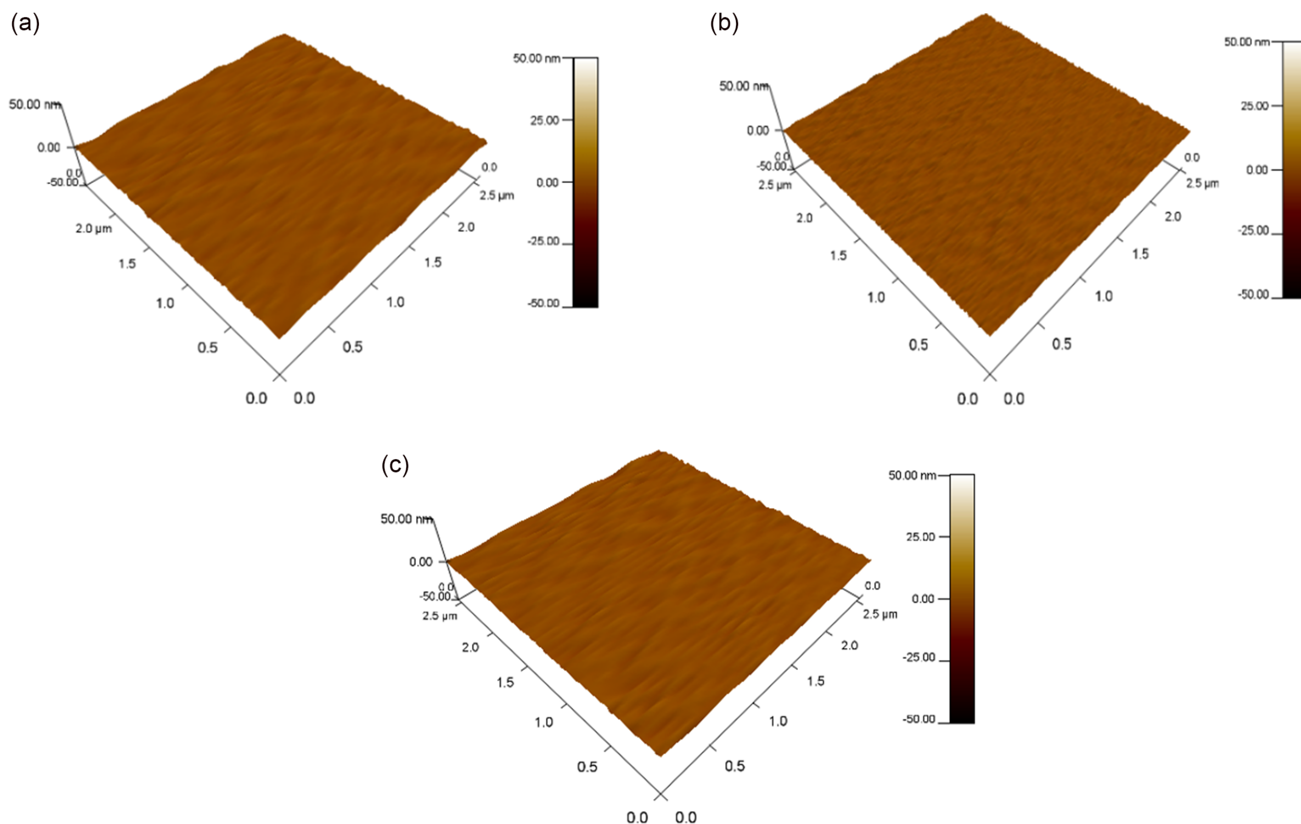


**Figure 7**
**30 MeV I Ion trajectory in GaAs single crystal**

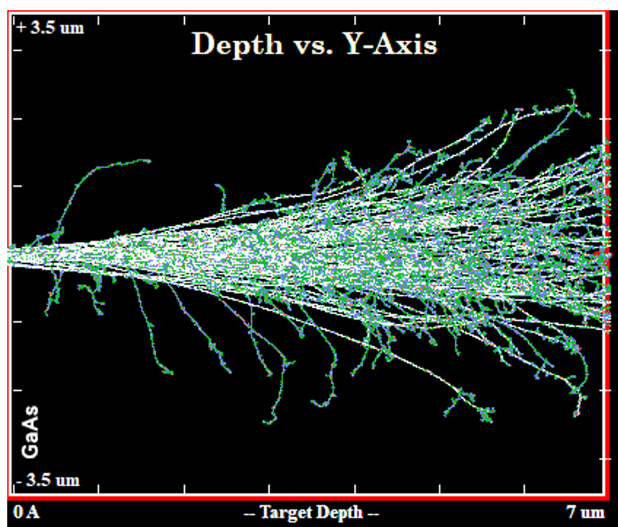


**Figure 8**
**1.16 GeV AU Ion trajectory in GaAs single crystal**

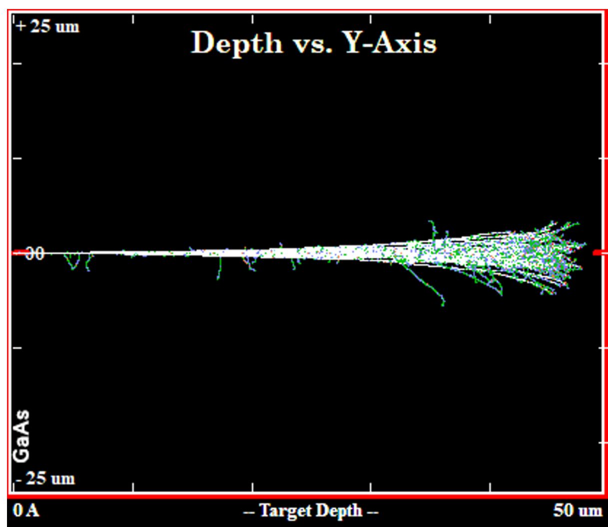


decrease of approximately 11 $cm^{-1}$ and 10 $cm^{-1}$. Similarly, Figure 12 shows the Raman spectra for pristine and I-irradiated GaAs samples, with the LO and TO modes in the pristine sample observed at 291.401 $cm^{-1}$ and 268.479 $cm^{-1}$. The downward shifts for ion fluences of $5 \times 10^{12}$ ions $cm^{-2}$ and $1 \times 10^{12}$ ions $cm^{-2}$ were 10 $cm^{-1}$ and 11 $cm^{-1}$, respectively. This phonon softening and broadening are attributed to the reduction in correlation length in semiconductor, which can be linked to phonon confinement in GaAs nanostructures [3]. A downward shift in Raman spectra of GaAs irradiated by I and Au ions has significant implications for photonics, as it reflects changes in the lattice dynamics and structural properties of the material induced by ion implantation.

**Figure 9**
**TRIM simulation for the distribution of vacancies (left) and energy loss (right) of GaAs irradiated with 1162.3 MeV AU ion**

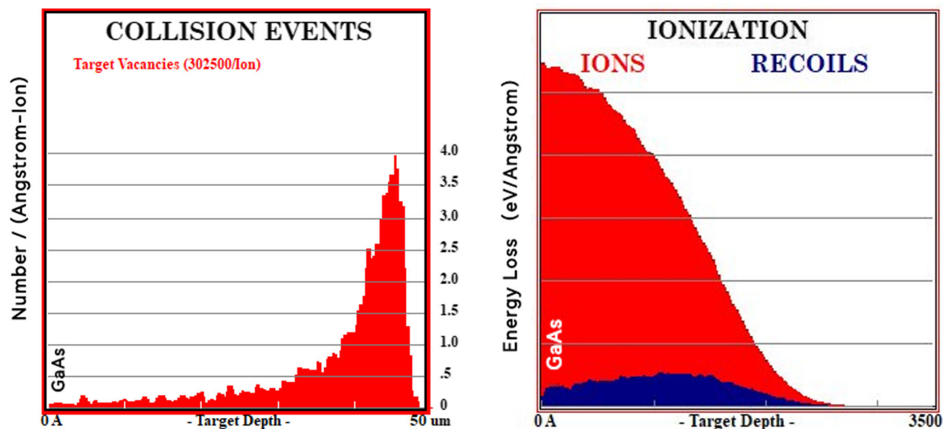


**Figure 10**
**TRIM simulation for the distribution of vacancies (left) and energy loss (right) of GaAs irradiated with 30 MeV I ion**

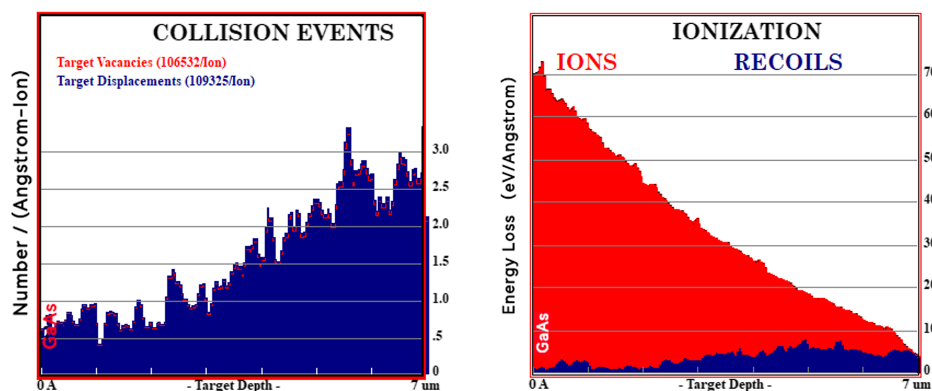


**Figure 11**
**Raman spectra of GaAs samples before and after irradiation with 1162.3 MeV Au ions at room temperature at varying fluence**

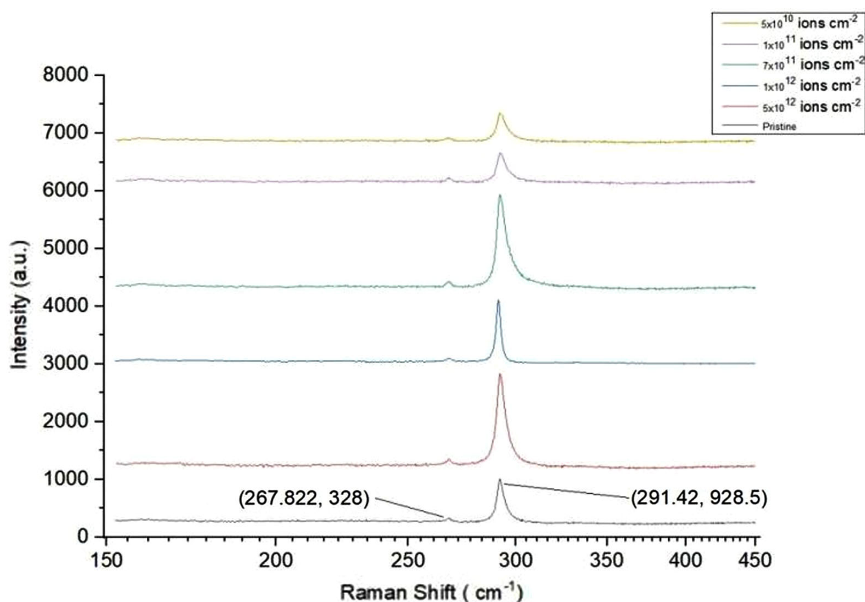

**Figure 12**
**Raman spectra of GaAs samples before and after irradiation with 30 MeV I ions at room temperature, analyzed at varying fluence**

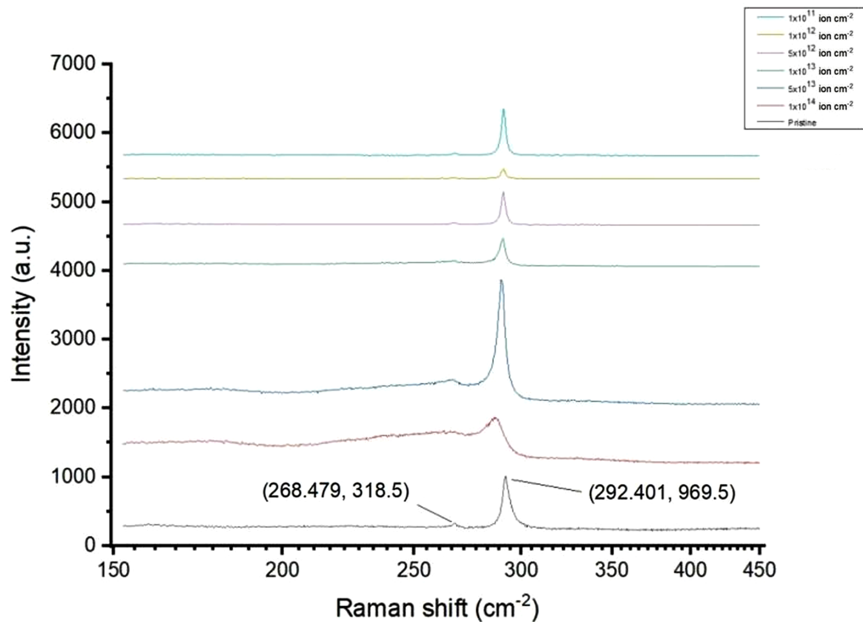


## 4. Conclusions

The surface modifications of GaAs irradiated with 1.16 GeV Au ions and 30 MeV I ions were analyzed using cutting-edge photonic and optical techniques, including atomic force microscopy and micro-Raman spectroscopy, across different ion fluence. The results demonstrate Au irradiation induced minimal nanostructure creation on the GaAs surface. However, the surface exhibited slight roughening due to ion irradiation, with a fluence-dependent increase in nanoscale surface roughness. Photonically-driven Raman spectroscopy revealed significant optical phonon softening, attributed to Phonon localization within the surface nanostructures. This confinement led to a pronounced downward shift in the LO and TO phonon modes in both I and Au-irradiated GaAs samples. These observations underscore the critical role of photonics in grasping the impact of ion irradiation, providing deep insights into the modulation of photonic characteristics through ion-induced surface modifications in semiconductor materials. Irradiating GaAs(100) with I and Au ions is crucial for tailoring its structural, electronic, and optical properties for advanced applications. One advantage includes the ability to create localized lattice defects and strain, enabling controlled modification of refractive indices for photonic devices such as waveguides. High-energy ions can also alter electronic properties, making GaAs suitable for quantum emitters and optoelectronic applications. And its drawback involves potential over-damage to the crystal lattice, leading to amorphization and a loss of useful optical or electronic properties. Additionally, excessive ion implantation can introduce unwanted scattering centers, reducing carrier mobility and device efficiency. Balancing ion energy and fluence is key to optimizing results.

## Ethical Statement

This study does not contain any studies with human or animal subjects performed by any of the authors.

## Conflicts of Interest

The authors declare that they have no conflicts of interest to this work.

## Data Availability Statement

Data are available from the corresponding author upon reasonable request.

## Author Contribution Statement

**Habib Abdurahman Arebu:** Conceptualization, Methodology, Software, Formal analysis, Resources, Data curation, Writing – original draft, Writing – review & editing, Visualization. **Omar Abdulsahib Saleh:** Writing – review & editing, Supervision.

## References

[1] Wesch, W., Kamarou, A., & Wendler, E. (2004). Effect of high electronic energy deposition in semiconductors. *Nuclear Instruments and Methods in Physics Research Section B: Beam Interactions with Materials and Atoms*, *225*(1–2), 111–128. https://doi.org/10.1016/j.nimb.2004.04.188

[2] Adeojo, S. A., Malherbe, J. B., Njoroge, E. G., Mlambo, M., Odutemowo, O. S., Thabethe, T. T., . . . , & Hlatshwayo, T. T. (2020). Effect of sequential isochronal annealing on the structure and migration behaviour of selenium-ion implanted in glassy carbon. *Vacuum*, *182*, 109689. https://doi.org/10.1016/j.vacuum.2020.109689

[3] Wang, Y. Y., Grygiel, C., Dufour, C., Sun, J. R., Wang, Z. G., Zhao, Y. T., . . . , & Toulemonde, M. (2014). Energy deposition by heavy ions: Additivity of kinetic and potential energy contributions in hillock formation on $CaF_2$. *Scientific Reports*, *4*(1), 5742. https://doi.org/10.1038/srep05742

[4] Wagner, M. F. P., Voss, K. O., Trautmann, C., & Toimil-Molares, M. E. (2023). Three-dimensional nanowire networks fabricated by ion track nanotechnology and their applications. *EPJ Techniques and Instrumentation*, *10*(1), 2. https://doi.org/10.1140/epjti/s40485-023-00090-9

[5] Ma, Y., Yang, Z., Gong, M., Gao, B., Li, Y., Lin, W., . . . , & Xia, Z. (2016). Swift heavy ion irradiation induced electrical degradation in deca-nanometer MOSFETs. *Nuclear Instruments and Methods in Physics Research Section B: Beam Interactions with Materials and Atoms*, *383*, 160–163. https://doi.org/10.1016/j.nimb.2016.07.007

[6] Lake, R. E., Persaud, A., Christian, C., Barnard, E. S., Chan, E. M., Bettiol, A. A., . . . , & Schenkel, T. (2021). Direct formation of nitrogen-vacancy centers in nitrogen doped diamond along the trajectories of swift heavy ions. *Applied Physics Letters*, *118*(8), 084002. https://doi.org/10.1063/5.0036643

[7] Golubenko, D. V., Yurova, P. A., Desyatov, A. V., Stenina, I. A., Kosarev, S. A., & Yaroslavtsev, A. B. (2022). Pore filled ion-conducting materials based on track-etched membranes and sulfonated polystyrene. *Membranes and Membrane Technologies*, *4*(6), 398–403. https://doi.org/10.1134/S2517751622060026

[8] Velişa, G., Zarkadoula, E., Iancu, D., Mihai, M. D., Grygiel, C., Monnet, I., . . . , & Weber, W. J. (2021). Near-surface modification of defective $KTaO_3$ by ionizing ion irradiation. *Journal of Physics D: Applied Physics*, *54*(37), 375302. https://doi.org/10.1088/1361-6463/ac0b11

[9] Jagerová, A., Mikšová, R., Romanenko, O., Plutnarova, I., Sofer, Z., Slepička, P., . . . , & Macková, A. (2021). Surface modification by high-energy heavy-ion irradiation in various crystalline ZnO facets. *Physical Chemistry Chemical Physics*, *23*(39), 22673–22684. https://doi.org/10.1039/D1CP02388H

[10] Moslem, W. M., El-Said, A. S., Morsi, S. A., Sabry, R., Yahia, M. E., El-Labany, S. K., & Bahlouli, H. (2019). On the formation of nanostructures by inducing confined plasma expansion. *Results in Physics*, *15*, 102696. https://doi.org/10.1016/j.rinp.2019.102696

[11] Gianuzzi, L. A., & Stevie, F. A. (2005). *Introduction to focused ion beams*. Germany: Springer.

[12] El-Said, A. S., Wilhelm, R. A., Heller, R., Facsko, S., Lemell, C., Wachter, G., . . . , & Aumayr, F. (2012). Phase diagram for nanostructuring $CaF_2$ surfaces by slow highly charged ions. *Physical Review Letters*, *109*(11), 117602. https://doi.org/10.1103/PhysRevLett.109.117602

[13] El-Said, A. S., Wilhelm, R. A., Heller, R., Ritter, R., Wachter, G., Facsko, S., . . . , & Aumayr, F. (2014). Nanostructuring $CaF_2$ surfaces with slow highly charged ions. *Journal of Physics: Conference Series*, *488*(1), 012002. https://doi.org/10.1088/1742-6596/488/1/012002

[14] Toulemonde, M., Benyagoub, A., Trautmann, C., Khalfaoui, N., Boccanfuso, M., Dufour, C., . . . , & Meftah, A. (2012). Dense and nanometric electronic excitations induced by swift heavy ions in an ionic $CaF_2$ crystal: Evidence for two thresholds of damage creation. *Physical Review B—Condensed Matter and Materials Physics*, *85*(5), 054112. https://doi.org/10.1103/PhysRevB.85.054112

[15] Manzoli, M., Freyria, F. S., Blangetti, N., & Bonelli, B. (2022). Brookite, a sometimes under evaluated $TiO_2$ polymorph. *RSC Advances*, *12*(6), 3322–3334. https://doi.org/10.1039/D1RA09057G

[16] Pankratova, V., Butikova, J., Kotlov, A., Popov, A. I., & Pankratov, V. (2024). Influence of swift heavy ions irradiation on optical and luminescence properties of $Y_3Al_5O_{12}$ single crystals. *Optical Materials: X*, *23*, 100341. https://doi.org/10.1016/j.omx.2024.100341

[17] Kumar, S., Kumawat, M. K., & Mohanty, T. (2023). Tailoring surface electronic properties of GO-$TiO_2$ hybrid nanostructures through interface modifications. *Applied Surface Science*, *609*, 155398. https://doi.org/10.1016/j.apsusc.2022.155398

[18] Rudzinska, P., Wawrzyniak, J., Grochowska, K., Karczewski, J., Ryl, J., & Siuzdak, K. (2023). Enhancing photoelectrochemical properties of titania nanotubes via rapid thermal annealing in hydrogen atmosphere. *Materials Science and Engineering: B*, *290*, 116324. https://doi.org/10.1016/j.mseb.2023.116324

[19] Isikgor, F. H., Zhumagali, S., T. Merino, L. V., De Bastiani, M., McCulloch, I., & De Wolf, S. (2023). Molecular engineering of contact interfaces for high-performance perovskite solar cells. *Nature Reviews Materials*, *8*(2), 89–108. https://doi.org/10.1038/s41578-022-00503-3

[20] Herweg, K., Nadig, V., Schulz, V., & Gundacker, S. (2023). On the prospects of $BaF_2$ as a fast scintillator for time-of-flight positron emission tomography systems. *IEEE Transactions on Radiation and Plasma Medical Sciences*, *7*(3), 241–252. https://doi.org/10.1109/TRPMS.2023.3237254

[21] Sato, Y., Koshikawa, H., Yamamoto, S., Sugimoto, M., Sawada, S. I., & Yamaki, T. (2021). Fabrication of size-and shape-controlled platinum cones by ion-track etching and electrodeposition techniques for electrocatalytic applications. *Quantum Beam Science*, *5*(3), 21. https://doi.org/10.3390/qubs5030021

[22] Okubo, N., Fujimura, Y., & Tomobe, M. (2021). Effect of irradiation on corrosion behavior of 316L steel in lead-bismuth eutectic with different oxygen concentrations. *Quantum Beam Science*, *5*(3), 27. https://doi.org/10.3390/qubs5030027

[23] Watanabe, H., Saita, Y., Takahashi, K., & Yasunaga, K. (2021). Desorption of implanted deuterium in heavy ion-irradiated zry-2. *Quantum Beam Science*, *5*(2), 9. https://doi.org/10.3390/qubs5020009

[24] Okuno, Y., & Okubo, N. (2021). Phase transformation by 100 keV electron irradiation in partially stabilized zirconia. *Quantum Beam Science*, *5*(3), 20. https://doi.org/10.3390/qubs5030020

[25] Ishikawa, N., Taguchi, T., & Ogawa, H. (2020). Comprehensive understanding of hillocks and ion tracks in ceramics irradiated with swift heavy ions. *Quantum Beam Science*, *4*(4), 43. https://doi.org/10.3390/qubs4040043

**How to Cite:** Arebu, H. A., & Saleh, O. A. (2025). Photonics-Driven Characterization of Highly Energetic Heavy Ion-Induced Modifications in GaAs Single Crystals Using Au and I Ions. *Journal of Optics and Photonics Research*. https://doi.org/10.47852/bonviewJOPR52024337